Published in final edited form as:
*Eur Radiol*. 2013 November ; 23(11): 2969–2978. doi:10.1007/s00330-013-2972-1.

# Breast MRI at 7 Tesla with a bilateral coil and T1-weighted acquisition with robust fat suppression: image evaluation and comparison with 3 Tesla

**Ryan Brown, PhD**[1], **Pippa Storey, PhD**[1], **Christian Geppert, PhD**[2], **KellyAnne McGorty, RT**[1], **Ana Paula Klautau Leite, MD**[1], **James Babb, PhD**[1], **Daniel K. Sodickson, MD, PhD**[1], **Graham C. Wiggins, DPhil**[1], and **Linda Moy, MD**[1]

[1]Bernard and Irene Schwartz Center for Biomedical Imaging, Department of Radiology, New York University Langone Medical Center, New York, NY, United States

[2]Siemens Medical Solutions USA Inc., New York, NY, United States

## Abstract

**Objectives—**To evaluate the image quality of T1-weighted fat-suppressed breast MRI at 7 T, and to compare 7-T and 3-T images.

**Methods—**Seventeen subjects were imaged using a 7-T bilateral transmit-receive coil and adiabatic inversion-based fat suppression (FS). Images were graded on a five-point scale and quantitatively assessed through signal-to-noise ratio (SNR), fibroglandular/fat contrast and signal uniformity measurements.

**Results—**Image scores at 7 T and 3 T were similar on standard-resolution images (1.1×1.1×1.1−1.6 $mm^3$), indicating that high-quality breast imaging with clinical parameters can be performed at 7 T. The 7-T SNR advantage was underscored on 0.6-mm isotropic images, where image quality was significantly greater than at 3 T (4.2 versus 3.1, $P \leq 0.0001$). Fibroglandular/fat contrast was more than two times higher at 7 T over 3 T, owing to effective adiabatic inversion-based FS and the inherent 7 T signal advantage. Signal uniformity was comparable at 7 T and 3 T ($P < 0.05$). Similar 7-T image quality was observed in all subjects, indicating robustness against anatomical variation.

**Conclusion—**The 7-T bilateral transmit-receive coil and adiabatic inversion-based FS technique mitigate the impact of high-field heterogeneity to produce image quality that is as good as or better than at 3 T

Corresponding Author: Ryan Brown, Ph.D., Bernard and Irene Schwartz Center for Biomedical Imaging New York University Langone Medical Center 660 First Avenue, Room 401 New York, NY, Tel: 212-263-3396, Fax: 212-263-7541, ryan.brown@nyumc.org.

Data in the current manuscript was presented in part in Brown, et. al, “Breast MRI at 7 Tesla with a Bilateral Coil and Robust Fat Suppression” in the Journal of Magnetic Resonance Imaging (accepted for publication, 2013).
While the JMRI manuscript indeed includes data from 11 of the 17 subjects presented in the current European Radiology submission, the JMRI manuscript focuses on 7T technical elements (such as the coil, transmit power limits, and B1+ calibration) as well as 7T advantages and hindrances. In contrast, the European Radiology submission focuses on the comparison between 3T and 7T (radiologist-based image quality metrics) and on the robustness of the 7T techniques to anatomic differences across subjects. As such, we believe that the added insight is worthy of a separate manuscript.

**Keywords**

high-field MRI; fat suppression; breast cancer; bilateral breast imaging; RF coil array

## INTRODUCTION

Breast magnetic resonance imaging (MRI) has been shown to be more sensitive to the detection of breast tumors than conventional investigations such as ultrasound or digital mammography. Mammography, the current standard for breast cancer screening, detects fewer than half of breast cancers in high-risk young women, in part because their increased breast density makes mammography less effective. MRI provides high-quality images regardless of breast density and enables small lesions to be visualized [1–2]. Dynamic T1-weighted acquisitions form the foundation of conventional breast MRI protocols and allow morphologic lesion assessment as well as time-course analysis of contrast uptake. Some morphological characteristics such as irregular margins can be less than 1 mm in dimension [3], suggesting that sub-millimetre spatial resolution is key to differentiation. Yet, spatial resolution of this order is rarely achieved in clinical MRI examinations due to signal-to-noise ratio (SNR) limitations. Breast MRI at high field (≥ 7 T) is driven by the promise of a greater signal-to-noise ratio (SNR), which could be traded for higher spatial resolution or faster acquisition times [4–8] to improve morphologically-based diagnosis or time-course analysis of the contrast enhancement, respectively. Another appealing aspect of high-field breast MRI is the potential to improve contrast between lesions and the background fat.

However, high-field breast MRI research is still in its infancy and is hampered by the lack of both commercially available radiofrequency (RF) coils and customized pulse sequences. Tailored RF coils are a critical determinant of SNR, signal uniformity, excitation (B1+) efficiency, and coverage. While high-density receive arrays have the potential to allow extremely fast acquisition and/or high spatial resolution [8], most 7 T studies have thus far been limited to unilateral coverage [4–5; 7–10]. Similarly, pulse sequence optimization is required to generate reliable tissue contrast in the presence of high-field difficulties such as increased B1+ and magnetic field (B0) heterogeneity. Low flip angle gradient echo-based T1-weighted sequences have been readily applied at 7 T due to their relative insensitivity to $B_1^+$ heterogeneity and low specific absorption rate (SAR) [11]. T2-weighted fast spin echo imaging has been more challenging due to high level of SAR associated with refocusing pulses and sensitivity to $B_1^+$ heterogeneity. Diffusion-weighted imaging has generally been impeded at high-field due to geometric distortion and short T2* associated with heterogeneous $B_0$. Recent advances indicate the potential to overcome these hurdles [4; 12], making a comprehensive high-field breast protocol within reach.

In this article, the main goal was to demonstrate three-dimensional (3D) T1-weighted 7 T breast imaging with a custom transmit-receive coil and adiabatic inversion-based fat-suppression (FS). The coil provided bilateral coverage while the FS technique was robust against B1+ heterogeneity. In evaluating 7 T T1-weighted images, we address the question of whether the potential high-field SNR and contrast advantages can be translated into improved image quality, FS efficacy, and image uniformity. Additionally, images were

evaluated with respect to anatomical and electrical breast properties, which are highly subject-dependent [13] and could be expected to have more influence on the resulting image quality at high field than at lower field. Finally, 7 T images were compared to familiar baseline measurements at 3 T in the same subjects.

## MATERIALS AND METHODS

### Subject cohort

Institutional Review Board approval was obtained for this Health Insurance Portability and Accountability Act (HIPAA)-compliant study. Seventeen asymptomatic subjects (age = 30 ± 7 years, age range = 19 to 46 years) underwent MRI without intravenous contrast material after written informed consent had been obtained. Subjects were imaged at arbitrary times with respect to their menstrual cycle. To reduce associated image variation, the interval between 7-T and 3-T examinations was as short as possible; the average delay between examinations was 3 ± 9 days. Both examinations were performed on the same day in 12 of the 17 subjects, while the intervals between examinations of the remaining subjects was 1, 2, 2, 8 and 40 days.

### MRI hardware

7-T images were acquired on a whole-body device (MAGNETOM, Siemens Healthcare, Erlangen, Germany) with maximum gradient amplitude of 40 mT $m^{-1}$ and a maximum slew rate of 150 $mT \cdot m^{-1} \cdot s^{-1}$. A custom bilateral two-channel coil was used for RF transmission and reception (Fig. 1). The coil consisted of two adjacent solenoids whose axes were perpendicular to the chest, with each solenoid enclosing one breast. Solenoids were chosen because of their high magnetic field uniformity, high efficiency, and convenient geometry to surround the breast and generate a linearly polarised magnetic field perpendicular to $B_0$. Passive tubular conductive RF shields were fitted around each solenoid to minimise coupling (< −30 dB), providing a high level of independence between the left and right elements. The 7-T coil had a 1.6-L aperture for each breast (15.5 cm in diameter, and 8.4 cm in height) and was housed in a repurposed shell that was originally designed for a 1.5-T clinical coil (utilised in Baltzer et al and Tozaki and Fukuma [14–15]). 7-T flip angle maps were acquired using the method described in Fautz et al [16].

3-T images were acquired on a Magnetom Tim Trio device (Siemens Healthcare) with the same gradient specifications as those listed for the 7-T system. At 3 T, the body coil provided RF excitation and a commercial bilateral seven-channel coil with aperture of 2.7 L per breast was used for RF reception (Invivo Corp., Gainsville, FL, USA).

### 3D T1-Weighted Fat-Suppressed Image Acquisition

3D T1-weighted gradient echo images were acquired using Siemens' volume interpolated breath-hold examination (VIBE). Three protocols were run, as detailed in Table 1: 1) to demonstrate feasibility, bilateral images were acquired at 7 T (transverse acquisition plane, 1.1 mm isotropic, 181 s acquisition time, parallel imaging acceleration rate = 2); 2) unilateral images were acquired for quantitative and qualitative assessment in the right breast at both 7 T and 3 T with "standard" resolution = 1.1 × 1.1 × 1.6 $mm^3$, acquisition time

= 71 s [3 T] and 119 s [7 T], and no parallel imaging acceleration and 3) “high” resolution images were acquired to exploit the 7 T SNR advantage (0.6 mm isotropic resolution, acquisition time = 324 s [3 T] and 390 s [7 T], and no parallel imaging acceleration). We point out that unilateral acquisitions were performed without parallel imaging acceleration in protocols 2 and 3 in order to simplify SNR analysis.

Fat suppression at 7 T was performed using spectrally selective adiabatic inversion recovery (SPAIR) due to its inherent robustness against $B_1^+$ heterogeneity. Two key modifications were made to adapt the 3-T product SPAIR module to 7-T: 1) the duration of the adiabatic pulse was reduced from 23 ms to 10 ms to match the increase in fat–water spectral separation, 2) the assumed T1 value of fat was increased to 540 ms based on preliminary phantom and in vivo measurements [1], and the inversion recovery duration was subsequently updated.

Although we found SPAIR to provide effective FS at 7 T, it should be noted that the technique prolongs acquisition time and is associated with a high specific absorption rate (SAR) due to its adiabatic pulse. SAR limits were obeyed by reducing the regularity with which the SPAIR module was applied from its default value of once per every 40 lines of acquired k-space to 60–100. This allowed the maximum flip angle within SAR limits to be roughly 15° for a TR of ~5 ms. At 3 T, where RF field heterogeneity is not so pronounced, we chose to maintain the chemical shift-based saturation method which is applied clinically at our institution (“quick fat saturation” on Siemens systems).

### Qualitative Image Assessment

Two radiologists with 12 and 4 years of breast MRI reading experience independently assessed 3D VIBE images. Images were presented such that the subject, sequence and field strength were randomised. The radiologists were blinded to sequence parameters and magnetic field strength, although 3-T and 7-T images could be distinguished by characteristic differences in signal strength. Image quality was rated on a scale of 1 to 5, with the following definitions: 1) non-diagnostic quality; little certainty in discerning fat and fibroglandular tissue due to strong artefacts including poor SNR or ineffective fat suppression. 2) poor image quality; difficult to make a diagnosis due to primarily indistinct borders between foci of fat and fibroglandular tissue. 3) acceptable image quality; able to make a diagnosis in a majority of the breast volume, though minor artefacts resulted in indistinct borders between foci of fat and fibroglandular tissue in some regions. 4) very good image quality; subjective certainty in making a correct assessment due to distinct borders between foci of fat and fibroglandular tissue and visualization of the underlying trabecular pattern. 5) excellent image quality; no artefacts, very easy to discern fat and fibroglandular tissue in the entire breast volume. The trabecular pattern along with cooper ligaments, milk ducts, and blood vessels were visualized. Finally, motion artefacts were noted as being present or absent.

### Quantitative Image Assessment

3D T1-weighted FS images were qualitatively assessed using the following metrics: SNR, fibroglandular/fat contrast, and signal uniformity. Images were exported from the scanner

console in standard format (DICOM; National Electrical Manufacturers Association, Rosslyn, Va) and converted into another format for semi-automated analysis (Matlab software [version 2009b, The MathWorks, Natick, MA, USA]). In each subject, measurements were made in a single slice near the centre of the breast. SNR was defined as $\mathbf{SNR}_{\mathrm{w}}=\frac{\overline{\mathbf{s}}_{\mathrm{w}}\mathbf{r}}{\boldsymbol{\sigma}_{\mathrm{n}}}$, where $\overline{s}_w$ is the mean signal intensity of the fibroglandular tissue, which was segmented from fat as described in the following paragraph. The noise $\sigma(n)$ was calculated from the standard deviation of the background intensity in magnitude sum-of-squares images, and $r$ is the correction factor necessary to account for the Rician noise distribution [17]. To remove bias due to sequence acquisition time $t$, normalised SNR values were reported: $\hat{SNR}_w=\frac{\overline{s}_w r}{\sigma_n\sqrt{t}}$. Fibroglandular/fat contrast was measured to assess FS efficacy: $c=\frac{\overline{s}_w-\overline{s}_f}{\overline{s}_w+\overline{s}_f}$, where $\overline{s}_f$ is the mean amplitude of the fat signal in adipose tissue following segmentation. Finally, signal uniformity was defined as: $u_w=\mathbf{1}-\frac{\sigma(s_w)}{\overline{s}_w}$, where $\sigma(s_w)$ is the standard deviation of the fibroglandular signal.

Fibroglandular tissue was segmented from fat in an automated fashion using the Dixon chemical species separation method [18–19]. For this purpose, an additional series of 2D gradient echo images was acquired in the central slice selected for quantitative image assessment (single sagittal slice, TR = 50 ms, TE = 2.7, 2.9, 3.1, 3.3 ms [7 T], TE = 3.5, 4.0, 4.5, 5.0 ms [3 T], flip angle = 20°, resolution = 0.7 × 0.7 $mm^2$, and slice thickness = 3 mm). The resulting fat/water maps were interpolated to match the spatial resolution of the VIBE images. Pixels with greater than 85% water or fat content were classified as fibroglandular or adipose tissue respectively (Fig. 2). A single manual step was performed by radiologist with 10 years' experience of breast MRI to exclude tissue posterior to the boundary between the breast and pectoralis muscle. ROIs were subsequently eroded by three pixels to reduce the likelihood of misregistration between Dixon and VIBE acquisitions.

Anatomical variability was assessed through two metrics: 1) bulk tissue composition was characterised by the Dixon-derived mean fat percentage value, and 2) breast volume was determined by contouring unilateral 3D T1-weighted image sets.

## Statistical Methods

Mixed model analysis of variance was used to assess and compare sequences in terms of the image quality scores and with respect to SNR, uniformity, and contrast. Generalised estimating equations based on a binary logistic regression model (a form of logistic regression for correlated data) were used to assess and compare sequences in terms of the prevalence of specific artefacts, as detected by the two readers. For all analyses, the intra-subject correlations imparted by the inclusion of multiple assessments per subject were accounted for by assuming data to be symmetrically correlated when acquired from the same subject and to be independent when derived for different subjects. The normality assumptions underlying the parametric analyses were found through residual plots and Shapiro-Wilk tests of residuals to be reasonably met. All statistical tests were conducted at the two-sided 5% significance level using SAS 9.3 (SAS Institute, Cary, NC, USA). Simple

kappa coefficients were used to assess inter-reader agreement. Kappa (K) was interpreted as an indication of poor agreement when less than zero, as slight agreement when $0 \leq K \leq 0.2$, as fair agreement when $0.2 < K \leq 0.4$, as moderate agreement when $0.4 < K \leq 0.6$ and as substantial agreement when $K > 0.6$.

## RESULTS

### Bilateral Imaging

The bilateral $B_1^+$ map in Fig. 3 shows adequate uniformity and good symmetry between $B_1^+$ fields in the left and right breasts. The high level of isolation between the left and right coil elements allowed straightforward application of bilateral imaging (Fig. 4). Fig. 4 illustrates good coverage, uniform fat suppression, and adequate penetration to visualise deep structures such as axillary lymph nodes. Sagittal views demonstrate excellent fat suppression throughout the breast volume, and particularly near the nipple and in the peripheral breast, where susceptibility gradients tend to be highest. Evidence of weak signal strength can be seen near the intersection of the inferior breast and chest wall because of a lack of coil coverage. All metrics indicated very good image quality: mean subjective score = 4.4, signal uniformity = 0.69±0.07, and fibroglandular/fat contrast = 0.71±0.05 (see Tables 2 and 3).

### Unilateral Imaging

A representative image set is shown in Fig. 5. At standard resolution ($1.1 \times 1.1 \times 1.6$ mm$^3$), the average image quality score was slightly higher at 7 T than at 3 T (see Table 2), although the difference was not statistically significant ($P = 0.27$). Despite high anatomical variability (breast volume = 675 ± 351 mL and Dixon-based fat composition = 66.5 ± 17.2%), no clear correlation was observed between image quality scores at 7 T and anatomical characteristics, indicating adequate insensitivity to tissue loading (Fig. 6 a and b).

High-resolution images (0.6 mm isotropic) underscore the 7-T SNR advantage and illustrate an exceptional level of fibroglandular tissue detail, such as ligaments and dendritic patterns that are difficult to visualise on standard-resolution images (Fig. 7). Furthermore, 3-T SNR was clearly too low to reliably identify structures on the high-resolution images. This was demonstrated in image quality scores, where high-resolution image quality was significantly lower at 3 T than at 7T (mean score of 4.2 at 7 T and 3.1 at 3 T, $P \leq 0.0001$). Low scores at 3 T were attributed to poor SNR, making fibroglandular tissue, particularly structural boundaries, difficult to visualise against the noisy background. Similarly, the low signal of fibroglandular tissue at 3 T accentuated the appearance of minor FS imperfections. Motion artefacts were noted in 2 of the 18 subjects at 7 T and none at 3 T.

Measured SNR at 7 T was more than five times higher than at 3 T, and fibroglandular/fat contrast was more than twice as high ($P < 0.0001$ in each case, see Table 3). Importantly, signal uniformity was similar at both fields ($P \geq 0.05$). 7-T fibroglandular/fat contrast and signal uniformity were independent of breast volume and fat composition (Fig. 6 e and g). A weak inverse relationship was observed between 7-T SNR and breast volume, likely because of increased tissue-related noise detected by the volume receive coil (Fig. 6 c). On the other hand, 3-T SNR was proportional to breast volume, likely because of the associated reduction

in distance between the tissue and the surface receive elements. Signal uniformity and fibroglandular/fat contrast were largely independent of spatial resolution (Table 3).

## DISCUSSION

This work demonstrates that breast MRI can be performed at 7 T with similar or better image quality than at 3 T. Although 7 T can be expected to provide a higher SNR, it also poses additional challenges in terms of RF and static field heterogeneity. Two technical developments were utilised to realise its full potential: 1) an efficient bilateral coil that provided adequate $B_1^+$ uniformity and high receive sensitivity, and 2) an adiabatic inversion-based fat suppression technique that provided effective and homogeneous nulling of adipose tissue. Good performance was demonstrated over a range of subjects and tissue loading conditions, which is especially important in high-field imaging, where anatomical variability is more likely to have an impact on image quality. This is a particularly pertinent consideration in breast imaging, where variability is more prominent than in other successful high-field applications such as brain or knee imaging.

Our data showed an approximately greater than five-fold gain in SNR at 7 T compared with 3 T. This is much higher than would be expected from the effect of spin polarisation, which is proportional to $B_0$. Clearly coil design also affects SNR and was not identical at 7 T and 3 T. However, it should be pointed out that the 3-T coil was a widely-utilised commercial coil, and, as such, was considered an appropriate reference. One way in which the design of the 7-T coil likely contributed to the SNR advantage was its smaller aperture. The 3-T coil utilised an “open” biopsy-compatible design, which required coil conductors to follow the edges of its rectangular aperture, thereby increasing the distance between conductors and tissue compared to a “closed” design. While a 3-T / 7-T comparison with identical RF coils would eliminate this variable, the design and construction of identical coils was beyond the scope of this work.

While the 7-T SNR advantage could be utilised for improved spatial or temporal resolution, we chose to focus on high spatial resolution. At 7-T, the 0.6-mm isotropic images allowed visualisation of dendritic patterns and ligaments that may be difficult to visualise at 3 T. This improvement at 7 T was reflected in significantly higher image quality scores for high-resolution imaging compared with 3 T. Although these results were obtained without intravenous contrast material, high-resolution 7-T breast imaging can be expected to improve lesion classification in contrast-enhanced examinations. Indeed, a strong correlation has been demonstrated between malignancy and morphological features such as clumped enhancement patterns and irregular or spiculated margins [20]. Detailed analysis of the margins of enhancing lesions and the internal architecture of mass and non-mass enhancement is limited to about 1 mm in-plane resolution and 2- to 3-mm slice thickness in conventional 1.5-T clinical dynamic protocols. Even with the improved spatial resolution available at 3 T, irregular mass borders can appear relatively smooth and a small carcinoma could present with benign imaging features. Additionally, prolonged baseline T1 relaxation at high field may accentuate differences between enhancing and non-enhancing tissue, thereby improving lesion conspicuity on subtracted images [21–22]. We are performing an

ongoing study to determine if the higher spatial resolution achievable at 7 T increases the ability to discriminate between benign and malignant masses.

Fat suppression can be challenging at 7 T owing to technical hurdles stemming from heterogeneous $B_0$ and $B_1^+$. For example, $B_0$ heterogeneity can be problematic in breast imaging because of the off-isocenter field-of-view and the strong dephasing associated with air/tissue interfaces, while $B_1^+$ heterogeneity can cause inconsistent saturation. To overcome these difficulties, we utilised SPAIR FS because its adiabatic pulse provides inherent robustness against $B_1^+$ heterogeneity. To mitigate the impact of $B_0$ heterogeneity, the bandwidth of the adiabatic pulse was broadened to 1 kHz, which was allowed by the increased fat/water spectral separation at 7 T. In combination with the inherently high fibroglandular signal strength at 7 T, SPAIR FS provided a greater than two-fold gain in fibroglandular/fat contrast over 3 T. Increased contrast was found to improve delineation of fibroglandular tissue borders, which, along with high spatial resolution available at 7 T, can be expected to improve lesion conspicuity.

Most 7-T breast studies have been limited to unilateral coverage owing to the lack of an appropriate bilateral coil. A bilateral 7-T breast coil can be difficult to design because of the desired high level of efficiency and $B_1^+$ uniformity over a relatively large field-of-view (~ 340 mm). This difficulty was overcome by utilising a 7-T bilateral coil that, in effect, comprised two identical and isolated (shielded) unilateral coils, each with a reduced field-of-view covering only the left or right breast. In other words, local excitation generated by each coil ensured that $B_1^+$ distortion (due to the short RF wavelength) was primarily limited to the given breast. In this way, the high uniformity and fat/water contrast achieved in unilateral imaging was trivially translated into roughly identical performance in bilateral acquisitions. This is a distinct advantage over conventional breast MRI at 3 T, where both breasts, and perhaps more importantly, the torso, lungs, and arms distort the $B_1^+$ field generated by the fully encompassing body coil. Recent reports have pointed out that complex RF interference patterns created by the body coil manifest as bimodal and heterogeneous $B_1^+$ distribution in the breasts [23–26], which results in inconsistent FS, variable enhancement ratio, and a possible reduction in lesion conspicuity.

We point out three concerns regarding the 3-T / 7-T image comparison: 1) As noted above, the smaller aperture of the 7-T coil likely accentuated the SNR advantage over 3 T. 2) Another concern is the inversion recovery period required by the 7-T SPAIR FS technique, which increased acquisition time by a factor of 1.2 to 1.7 over 3-T saturation-based FS acquisitions (Table 1). As a longer acquisition time can in principle be used to improve signal, the reported SNR values were normalised by the total acquisition time to avoid bias. However, it should be borne in mind that acquisition time is also important for the evaluation of contrast medium uptake in dynamic imaging. Although we did not administer intravenous contrast material in this study, the bilateral and standard-resolution 7-T VIBE sequences fall within typical dynamic acquisition times, while the high-resolution unilateral sequence would require a parallel imaging acceleration factor of 2–3 to provide adequate temporal resolution. A unilateral accelerated acquisition necessitates a high-channel receive array such as those demonstrated by van de Bank et al [8] and Nnewihe et al.[27]. 3) The improvement in fibroglandular/fat contrast at 7 T was largely attributed to improved fat

suppression with the SPAIR technique. While it was crucial to use SPAIR at 7 T because of $B_1^+$ heterogeneity, this was not the case at 3 T, and we chose instead to follow the standard clinical protocol at our institution, which employed chemical shift-based fat saturation. The use of SPAIR at 3 T might improve fibroglandular/fat contrast to a level approaching that achieved at 7 T, but would slightly increase the imaging time as described above. Furthermore, our results showed high signal uniformity at 7 T, which is likely attributable to the dual-solenoid coil and the 3D GRE acquisition. Although, we acknowledge that there was low signal in the posterior breast, as illustrated in Fig. 4. This could potentially be addressed with a straightforward modification to a future 7-T dual-solenoid coil that is tapered to a larger diameter near the chest wall.

In conclusion, by addressing 7-T technical concerns through a bilateral transmit-receive coil and robust FS technique, excellent T1-weighted image quality, signal uniformity and FS were demonstrated in a range of subjects with widely varying anatomy. 7-T image quality was equal to that of 3T on standard-resolution images, and showed a clear advantage of visualising fibroglandular tissue detail on high-resolution images (0.6 mm isotropic). While we have focused on a T1-weighted GRE sequence, we acknowledge that a fully functional protocol for bilateral contrast enhanced breast MRI at 7 T requires additional effort to establish T2-weighted fast spin echo and diffusion-weighted sequences. T2-weighted acquisitions must overcome difficulties associated with SAR, T2 blurring, and heterogeneous FS, while diffusion sequences must overcome spatial distortion, T2* blurring, and heterogeneous FS. Recent literature suggests that 7 T protocols will soon provide a sufficient variety of tissue contrast to support clinical translation [4; 12].

## Acknowledgments

This work was funded in part by NIH grant R01 EB002568. Christian Geppert is an employee of Siemens.

## References

1. Brown, R.; McGorty, K.; Moy, L.; DeGregorio, S.; Sodickson, DK.; Wiggins, GC. Sub-Millimeter Breast Imaging and Relaxivity Characterization at 7T. ISMRM; Montreal, Canada: 2011. p. 3092
2. Brown, R.; Storey, P.; McGorty, K., et al. Toward improved T1-weighted breast imaging at 7T: preliminary results and comparison with 3T. ISMRM; Melbourne, Australia: 2012. p. 2981
3. Kuhl CK. Breast MR imaging at 3T. Magn Reson Imaging Clin N Am. 2007; 15:315–320. [PubMed: 17893052]
4. Korteweg MA, Veldhuis WB, Visser F, et al. Feasibility of 7 Tesla breast magnetic resonance imaging determination of intrinsic sensitivity and high-resolution magnetic resonance imaging, diffusion-weighted imaging, and (1)H-magnetic resonance spectroscopy of breast cancer patients receiving neoadjuvant therapy. Invest Radiol. 2011; 46:370–376. [PubMed: 21317792]
5. Umutlu L, Maderwald S, Kraff O, et al. Dynamic contrast-enhanced breast MRI at 7 Tesla utilizing a single-loop coil: a feasibility trial. Acad Radiol. 2010; 17:1050–1056. [PubMed: 20599158]
6. Lee, RF.; Moy, L.; Brown, R., et al. 7T high resolution breast MRI. ISMRM; Seattle, WA: 2006. p. 2900
7. Stehouwer BL, Klomp DWJ, Korteweg MA, et al. 7 T versus 3 T contrast-enhanced breast Magnetic Resonance Imaging of invasive ductulolobular carcinoma: First clinical experience. Magn Reson Imaging.
8. van de Bank BL, Voogt IJ, Italiaander M, et al. Ultra high spatial and temporal resolution breast imaging at 7T. NMR Biomed. 2013; 26:367–375.

9. Stehouwer, BL.; Klomp, DWJ.; Luijten, PR., et al. Feasibility of contrast-enhanced and high-resolution 7 Tesla MRI in patients with suspicious breast lesions. ISMRM; Melbourne, Australia: 2012. p. 1474
10. Stehouwer, BL.; Klomp, DWJ.; Luijten, PR.; Mali, WPTM.; van den Bosch, MAAJ.; Veldhuis, WB. Dynamic contrast-enhanced MRI of the breast at 7T and 3T; initial results of an intra-individual comparison of BI-RADS-MRI lesion assessment. ISMRM; Melbourne, Australia: 2012. p. 1485
11. Stehouwer BL, Klomp DW, Korteweg MA, et al. 7 T versus 3T contrast-enhanced breast magnetic resonance imaging of invasive ductulolobular carcinoma: first clinical experience. Magn Reson Imaging. 2013; 31:613–617. [PubMed: 23116848]
12. Zaric, O.; Pinker, K.; Gruber, S., et al. Diffusion Weighted Imaging of the Breast at 7T – Ready for Clinical Application?. ISMRM; Salt Lake City, Utah: 2013. p. 196
13. Lazebnik M, Popovic D, McCartney L, et al. A large-scale study of the ultrawideband microwave dielectric properties of normal, benign and malignant breast tissues obtained from cancer surgeries. Phys Med Biol. 2007; 52:6093–6115. [PubMed: 17921574]
14. Tozaki M, Fukuma E. 1H MR spectroscopy and diffusion-weighted imaging of the breast: are they useful tools for characterizing breast lesions before biopsy? AJR Am J Roentgenol. 2009; 193:840–849. [PubMed: 19696300]
15. Baltzer PA, Dietzel M, Burmeister HP, et al. Application of MR mammography beyond local staging: is there a potential to accurately assess axillary lymph nodes? evaluation of an extended protocol in an initial prospective study. Am J Roentgenol. 2011; 196:W641–647. [PubMed: 21512057]
16. Fautz, HP.; Vogel, M.; Gross, P.; Kerr, A.; Zhu, Y. B1 mapping of coil arrays for parallel transmission. ISMRM; Toronto, Ontario: 2008. p. 1247
17. Constantinides CD, Atalar E, McVeigh ER. Signal-to-noise measurements in magnitude images from NMR phased arrays. Magn Res Med. 1997; 38:852–857.
18. Reeder SB, Wen Z, Yu H, et al. Multicoil Dixon chemical species separation with an iterative least-squares estimation method. Magn Reson Med. 2004; 51:35–45. [PubMed: 14705043]
19. Glover GH, Schneider E. Three-point Dixon technique for true water/fat decomposition with B0 inhomogeneity correction. Magn Reson Med. 1991; 18:371–383. [PubMed: 2046518]
20. Mahoney MC, Gatsonis C, Hanna L, DeMartini WB, Lehman C. Positive predictive value of BI-RADS MR imaging. Radiology. 2012; 264:51–58. [PubMed: 22589320]
21. Krautmacher C, Willinek WA, Tschampa HJ, et al. Brain tumors: full- and half-dose contrast-enhanced MR imaging at 3.0 T compared with 1.5 T–Initial Experience. Radiology. 2005; 237:1014–1019. [PubMed: 16237142]
22. Elster AD. How much contrast is enough? Dependence of enhancement on field strength and MR pulse sequence. Eur Radiol. 1997; 7(Suppl 5):276–280. [PubMed: 9370559]
23. Kuhl CK, Kooijman H, Gieseke J, Schild HH. Effect of B1 inhomogeneity on breast MR imaging at 3.0 T. Radiology. 2007; 244:929–930. [PubMed: 17709843]
24. Azlan CA, Di Giovanni P, Ahearn TS, Semple SI, Gilbert FJ, Redpath TW. B1 transmission-field inhomogeneity and enhancement ratio errors in dynamic contrast-enhanced MRI (DCE-MRI) of the breast at 3T. J Magn Reson Imaging. 2010; 31:234–239. [PubMed: 20027594]
25. Sung K, Daniel BL, Hargreaves BA. Transmit B1+ field inhomogeneity and T1 estimation errors in breast DCE-MRI at 3 Tesla. J Magn Reson Imaging.
26. Hancu I, Lee SK, Dixon WT, et al. Field shaping arrays: a means to address shading in high field breast MRI. J Magn Reson Imaging. 2012; 36:865–872. [PubMed: 22730242]
27. Nnewihe AN, Grafendorfer T, Daniel BL, et al. Custom-fitted 16-channel bilateral breast coil for bidirectional parallel imaging. Magn Reson Med. 2011; 66:281–289. [PubMed: 21287593]

**Key points**

- High image quality bilateral breast MRI is achievable with clinical parameters at 7 T.
- 7-T high-resolution imaging improves delineation of subtle tissue structures.
- Adiabatic-based fat suppression provides excellent fibroglandular/fat contrast at 7 T.
- 7-T and 3-T 3D T1-weighted gradient echo imaging have similar signal uniformity.
- The 7-T dual solenoid coil enables bilateral imaging without compromising uniformity.


**Fig. 1.**

Photograph of the 7-T bilateral coil: (a) dual solenoid with the cover and shield removed, (b) dual solenoid with shield, and (c) assembled coil

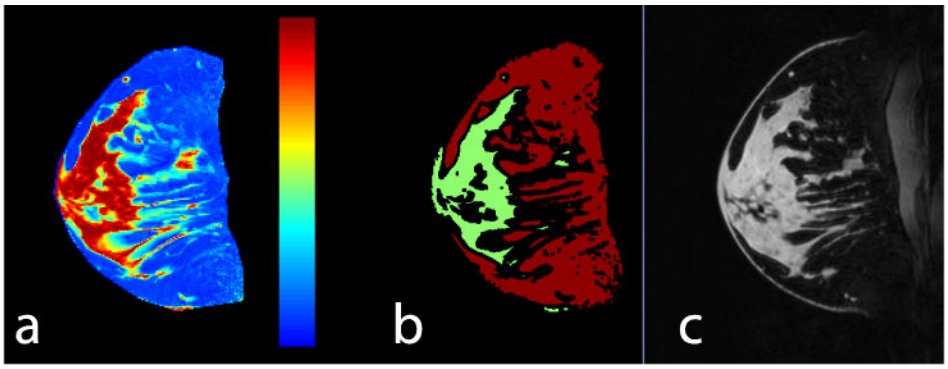


**Fig. 2.**

A water map (a) was used to generate masks of fat (red) and water (green) (b) in which corresponding 7-T T1-weighted fat-suppressed (FS) images were evaluated (c)

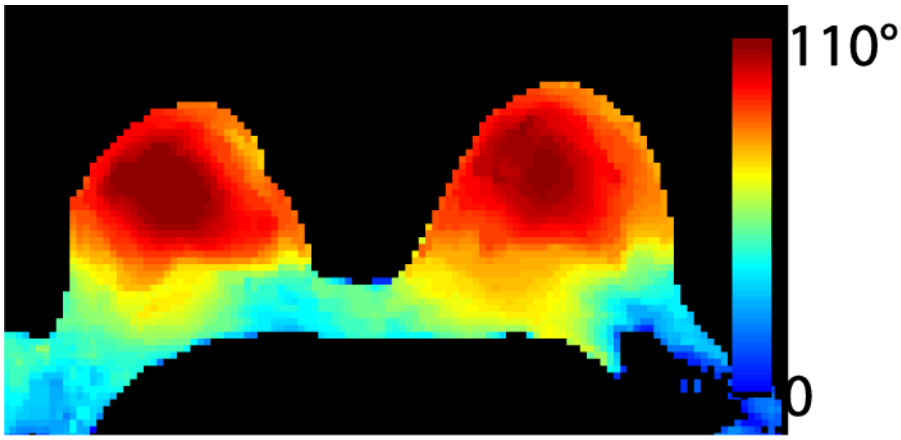


**Fig. 3.**

The bilateral flip angle map demonstrates symmetric excitation in the left and right breasts. Flip angle uniformity was 75% in a region-of-interest encompassing both breasts to the pectoralis muscle. One limitation of the local transmit coil is the relatively weak level of excitation posterior to the pectoralis muscle which could limit signal in the lymph nodes

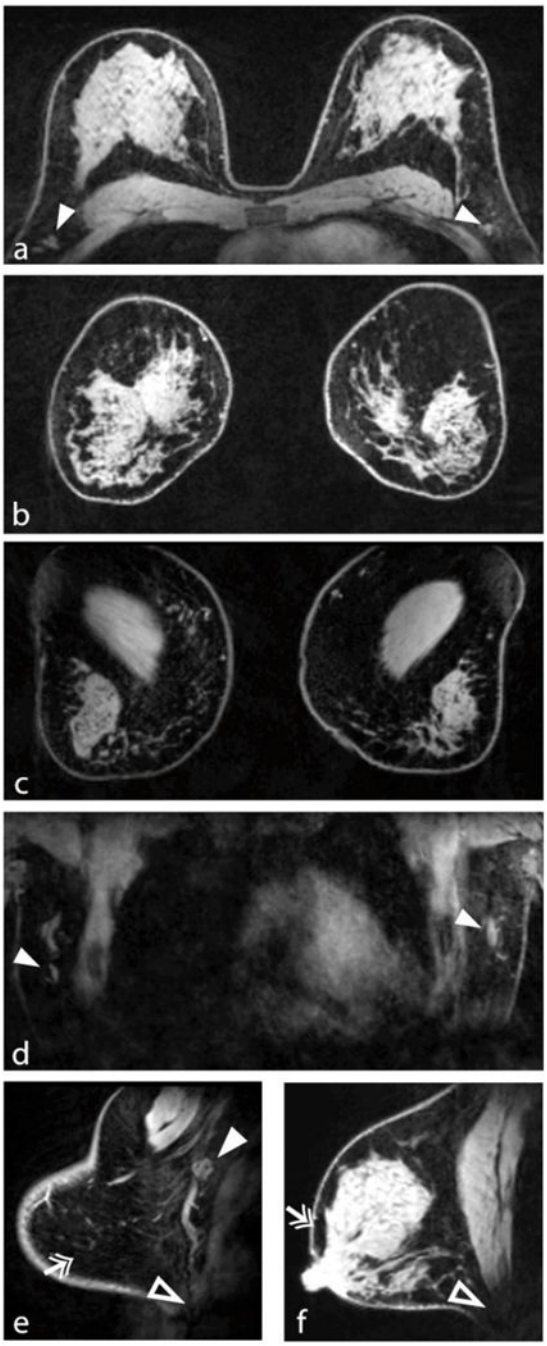


**Fig. 4.**

Demonstration of 7-T bilateral breast imaging. The transverse and reformatted coronal views (a, b) illustrate good coverage and uniform fat suppression. Coronal views through the chest wall (c) and anterior heart (d) demonstrate adequate penetration for visualisation of deep structures such as the pectoralis muscle and lymph nodes (solid arrowheads). Sagittal views demonstrate excellent fat suppression (double arrows) at the breast periphery (e) and near the nipple (f), which are areas that can be problematic owing to high susceptibility

gradients. Signal at the intersection of the inferior breast and chest wall was limited because of a lack of coil coverage (open arrowheads in e and f)

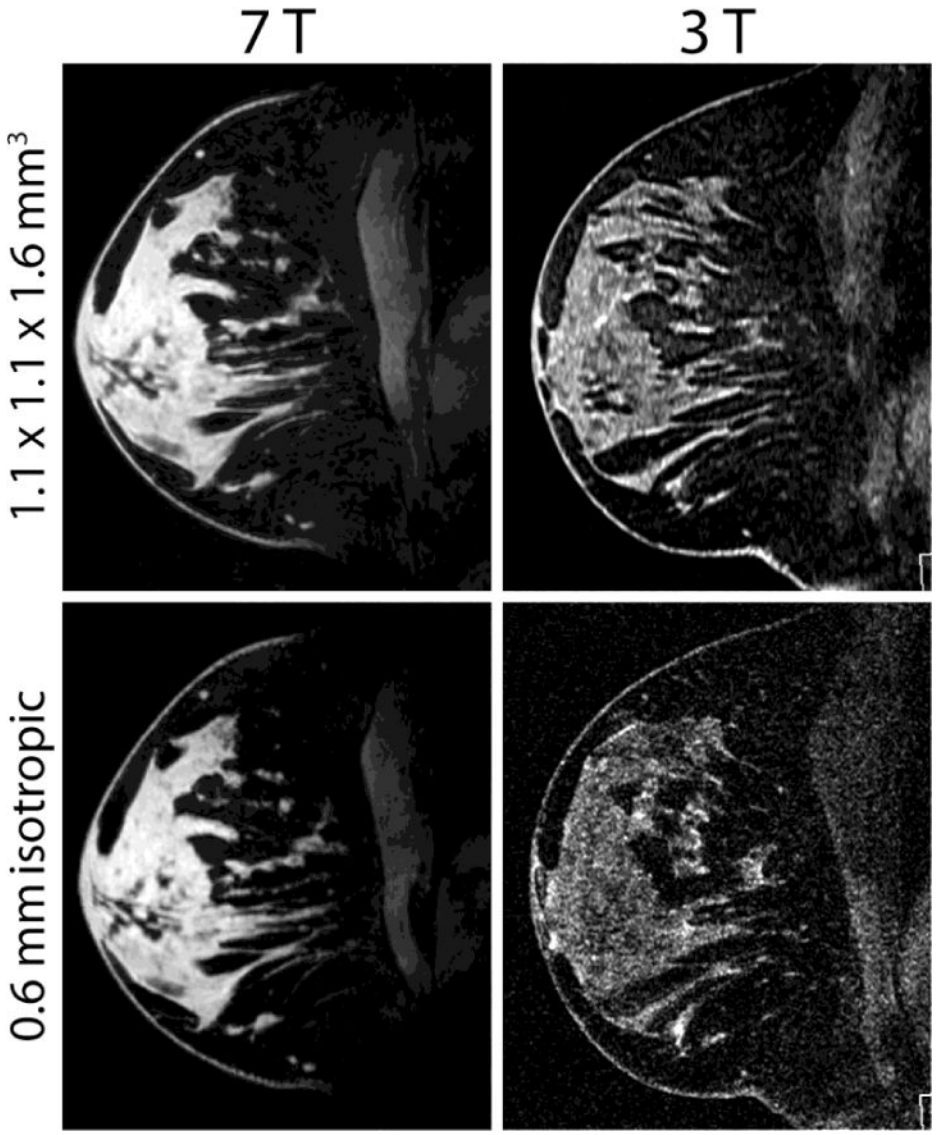


**Fig. 5.**

Representative standard and high-resolution T1-weighted FS images acquired at 7 T and 3 T in the same subject A clear SNR and image quality advantage can be appreciated in the 7 T images.

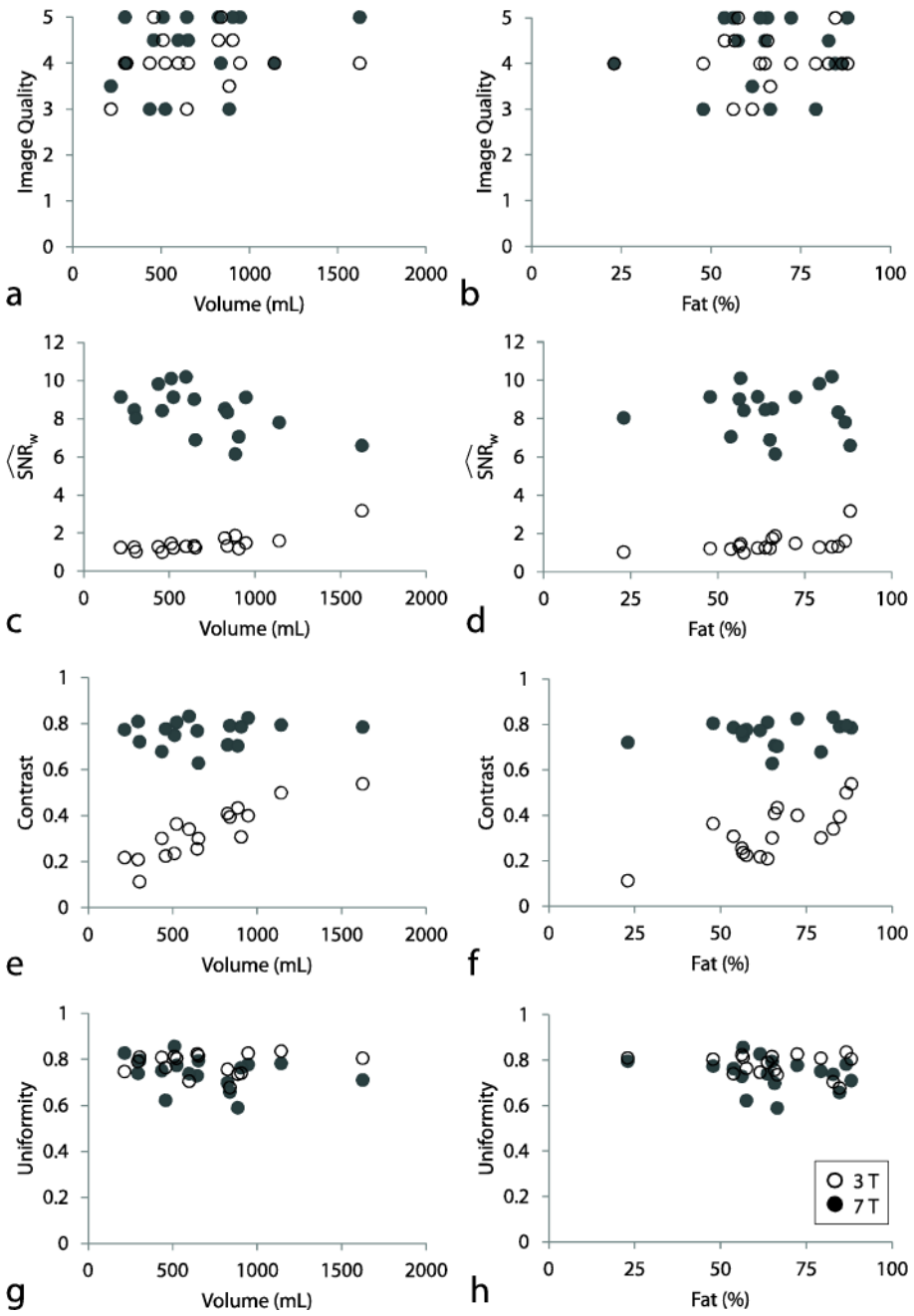


**Fig. 6.**

Standard-resolution image quality metrics at 7 T (solid circles) and 3 T (empty circles) as a function of anatomical characteristics; breast volume (left column) and fat percentage (right column). Aside from a weak inverse relationship between 7-T SNR and breast volume, 7-T image metrics were consistent across subjects and showed little correlation with anatomical characteristics

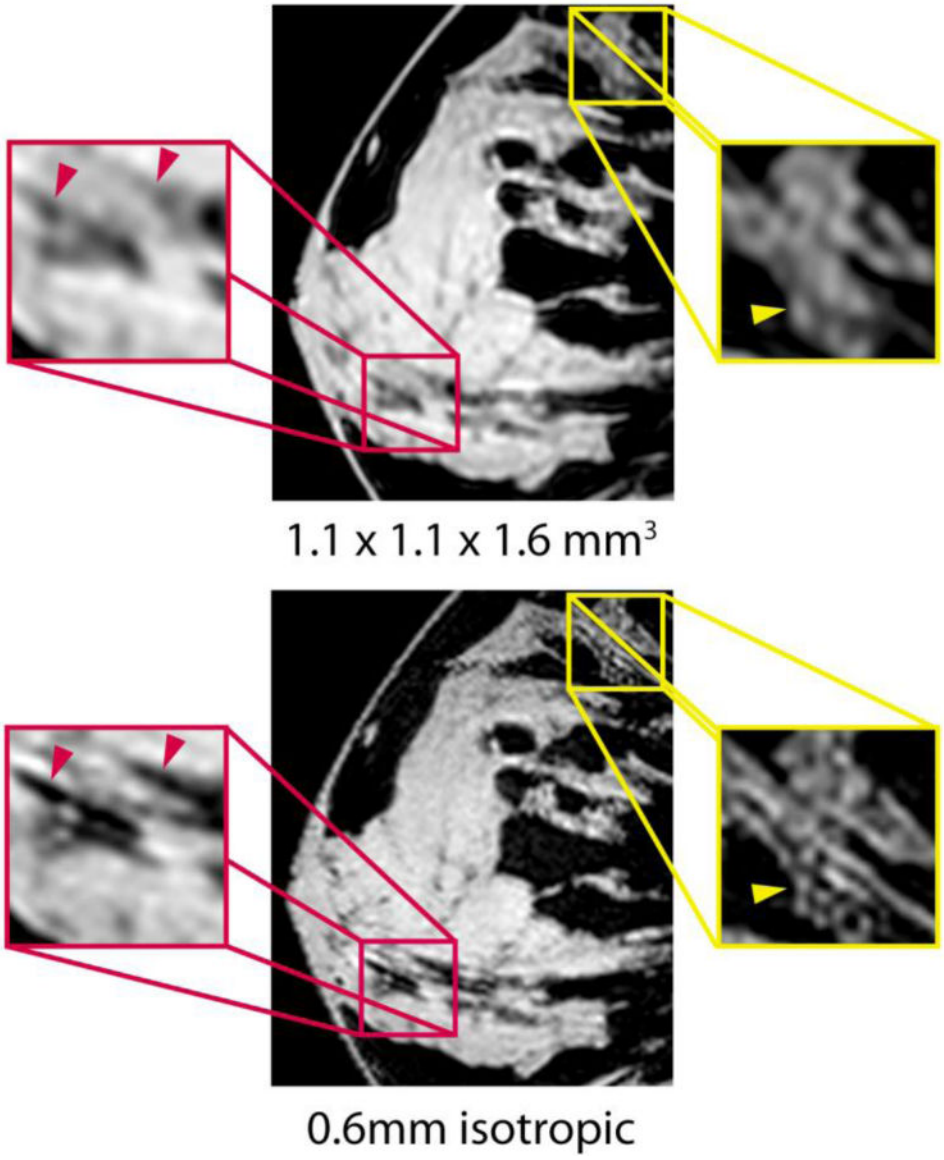


**Fig. 7.**

Representative standard (top) and high (bottom) resolution 7-T T1-weighted FS images acquired in the same subject. Enlarged sagittal views illustrate the high level of fibroglandular detail at 7 T. Ligaments (red arrowheads) and dendritic architecture (yellow arrowheads) can be visualised on 7-T high-resolution images, but are blurred on 7-T standard-resolution images

**Table 1**

3D T1-weighted fat-suppressed (FS) pulse sequence parameters

| Sequence description | Bilateral | Standard resolution | | High resolution | |
|---|---|---|---|---|---|
| Field strength (T) | 7 | 3 | 7 | 3 | 7 |
| FS method | SPAIR | Saturation | SPAIR | Saturation | SPAIR |
| TE (ms) | 1.9 | 1.47 | 2.14 | 1.78 | 2.75 |
| TR (ms) | 4.2 | 3.78 | 4.52 | 4.39 | 5.36 |
| Nominal flip angle (°) | 10* | 12 | 5–10* | 12 | 5* |
| Bandwidth (Hz/pixel) | 540 | 543 | 545 | 539 | 540 |
| FS lines per shot | 100 | 40 | 60 | 224 | 100 |
| Acquisition time (s) | 181 | 71 | 119 | 324 | 390 |
| Number of slices | 144 | 144 | 144 | 224 | 208 |
| Field-of-view ($mm^2$) | 310 × 310 | 190 × 190 | 190 × 190 | 190 × 190 | 190 × 190 |
| Acquisition matrix | 288 × 288 | 176 × 176 | 174 × 174 | 320 × 320 | 320 × 320 |
| Acquired voxel size ($mm^3$) | 1.1 × 1.1 × 1.1 | 1.1 × 1.1 × 1.6 | 1.1 × 1.1 × 1.6 | 0.6 × 0.6 × 0.6 | 0.6 × 0.6 × 0.6 |
| Parallel imaging acceleration | 2 | 1 | 1 | 1 | 1 |

SPAIR spectrally selective adiabatic inversion recovery

*7-T flip angles were calibrated in the peripheral fat tissue to ensure efficacy of the SPAIR module. The flip angle in the centre of the breast is expected to be approximately 25% greater.

**Table 2**

Summary of image quality scores

| Sequence description | Standard resolution | | High resolution | | Bilateral |
|---|---|---|---|---|---|
| Field strength (T) | 3 | 7 | 3 | 7 | 7 |
| Number of subjects | 17 | | 16 | | 5 |
| Image quality (reader 1) | 4.0±0.6 | 4.3±0.9 | 3.3±0.7 | 4.2±0.7 | 4.4±0.5 |
| *P* value | 0.27 | | 0.0001 | | |
| Image quality (reader 2) | 4.1±0.6 | 4.2±0.8 | 2.9±0.8 | 4.1±0.8 | 4.4±0.9 |
| *P* value | 0.64 | | <0.0001 | | |
| Reader agreement (kappa value) | 0.47 | 0.67 | 0.45 | 0.87 | * |

The scoring system is defined as: 1) non-diagnostic quality; little certainty in discerning fat and fibroglandular tissue due to strong artefacts including poor SNR or ineffective fat suppression. 2) poor image quality; difficult to make a diagnosis due to primarily indistinct borders between foci of fat and fibroglandular tissue. 3) acceptable image quality; able to make a diagnosis in a majority of the breast volume, though minor artefacts resulted in indistinct borders between foci of fat and fibroglandular tissue in some regions. 4) very good image quality; subjective certainty in making a correct assessment due to distinct borders between foci of fat and fibroglandular tissue and visualization of the underlying trabecular pattern. 5) excellent image quality; no artefacts, very easy to discern fat and fibroglandular tissue in the entire breast volume. The trabecular pattern along with cooper ligaments, milk ducts, and blood vessels were visualized.

*Not calculated due to small sample size.

**Table 3**

Summary of quantitative metrics

| Sequence description | Standard resolution | | High resolution | | Bilateral |
|---|---|---|---|---|---|
| Field strength (T) | 3 | 7 | 3 | 7 | 7 |
| Number of subjects | 17 | | 16 | | 5 |
| $\hat{SNR}_w$ | 1.45±0.48 | 8.15±1.60 | 0.28±0.12 | 1.87±0.35 | Not measured |
| *P* value | <0.0001 | | <0.0001 | | |
| Contrast (*c*) | 0.33±0.11 | 0.75±0.08 | 0.28±0.08 | 0.70±0.09 | 0.71±0.05 |
| *P* value | <0.0001 | | <0.0001 | | |
| Uniformity ($u_w$) | 0.78±0.04 | 0.75±0.07 | 0.72±0.04 | 0.73±0.11 | 0.69±0.07 |
| *P* value | 0.05 | | 0.57 | | |